



Andreadis, K., Schumann, G., Stampoulis, D., Bates, P., Brackenridge, G. R., & Kettner, A. (2017). Can Atmospheric Reanalysis Data Sets Be Used to Reproduce Flooding Over Large Scales? *Geophysical Research Letters*.
<https://doi.org/10.1002/2017GL075502>

Peer reviewed version

Link to published version (if available):
[10.1002/2017GL075502](https://doi.org/10.1002/2017GL075502)

[Link to publication record in Explore Bristol Research](#)
PDF-document

This is the author accepted manuscript (AAM). The final published version (version of record) is available online via Wiley at <http://onlinelibrary.wiley.com/doi/10.1002/2017GL075502/full>. Please refer to any applicable terms of use of the publisher.

University of Bristol - Explore Bristol Research

General rights

This document is made available in accordance with publisher policies. Please cite only the published version using the reference above. Full terms of use are available:
<http://www.bristol.ac.uk/pure/about/ebr-terms>

Supporting Information for

“Can atmospheric reanalysis datasets be used to reproduce flooding over large scales?”

**Konstantinos M. Andreadis^{1*}, Guy J-P. Schumann^{2,3}, Dimitrios Stampoulis¹, Paul D. Bates³,
G. Robert Brakenridge⁴, Albert J. Kettner⁴**

¹Jet Propulsion Laboratory, California Institute of Technology, Pasadena, CA, USA

²Remote Sensing Solutions, Inc., Monrovia, CA, USA

³School of Geographical Sciences, University of Bristol, Bristol, UK

⁴Institute of Arctic and Alpine Research, University of Colorado, Boulder, CO, USA

Contents

1. Figures S1 to S8
2. Table S1

Introduction

This supplemental material provides Figures S1-S8 and Table S1. Figure S1 shows a comparison of the seasonal means of rainfall during 1998-2012 between the TRMM dataset and the downscaled data for each of the reanalysis products. Figure S2 shows an elevation map of the Australia domain, along with the modeled rivers and the boundary inflows and outflows. Figure S3 shows a Receiver Operating Characteristics (ROC) curve for the calibration of the LISFLOOD-FP model in terms of flood inundation in the Murray-Darling River basin. Figure S4 shows time series of boundary inflows from observations and the envelope of the ensemble simulations. Figures S5-S8 show zoomed versions of the bivariate choropleth maps of agreement in maximum inundation extent between the benchmark and reanalysis simulations. Table S1 shows the list of VIC model parameters that were sampled to create the ensemble simulations, and the range of values for each.

*4800 Oak Grove Dr.

M/S 300-320M

Pasadena, CA 91109

Corresponding author: Konstantinos Andreadis, kandread@jpl.nasa.gov

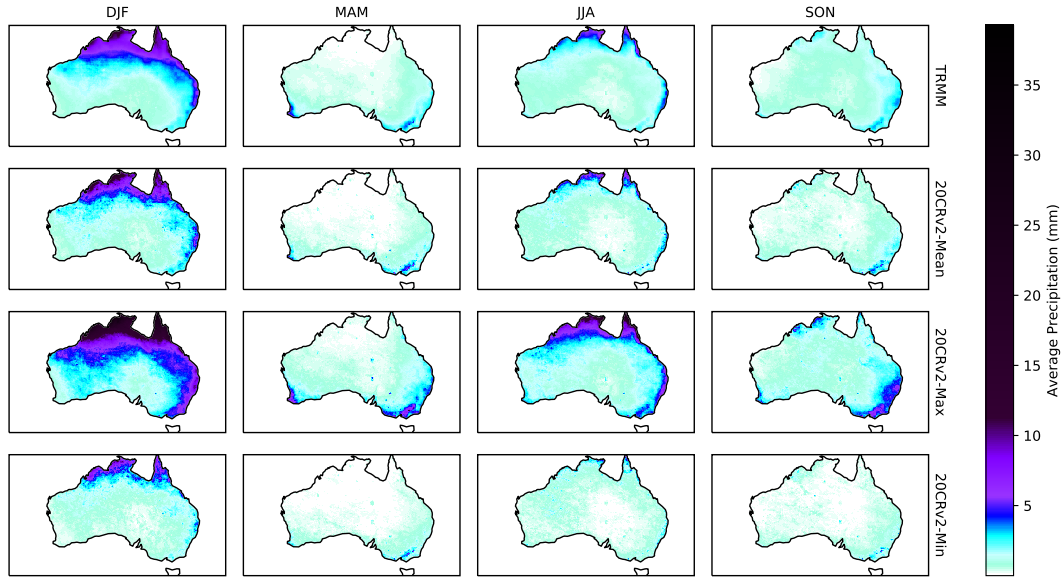


Figure S1. Comparison of precipitation seasonal means (1998-2012) derived by downscaling NCEP, JRA, MERRA, and ERA reanalysis data with TRMM observations.

Table S1. VIC model parameters used to generate ensemble simulations.

Parameter	Description	Range
$b_{infiltr}$	Variable infiltration curve parameter	(0, 0.4]
$D_{s,max}$	Maximum potential baseflow from the lowest soil layer (mm/day)	(0, 50]
D_s	Fraction of $D_{s,max}$ where nonlinear baseflow begins	(0, 1]
W_s	Maximum soil moisture fraction where nonlinear baseflow occurs	(0, 1]
$expt$	Exponent describing variation of hydraulic conductivity with soil moisture	[3.0, 30.0]
dz_2	Thickness of middle soil layer (m)	[0.2, 1.5]
dz_3	Thickness of bottom soil layer (m)	[1.5, 6.0]

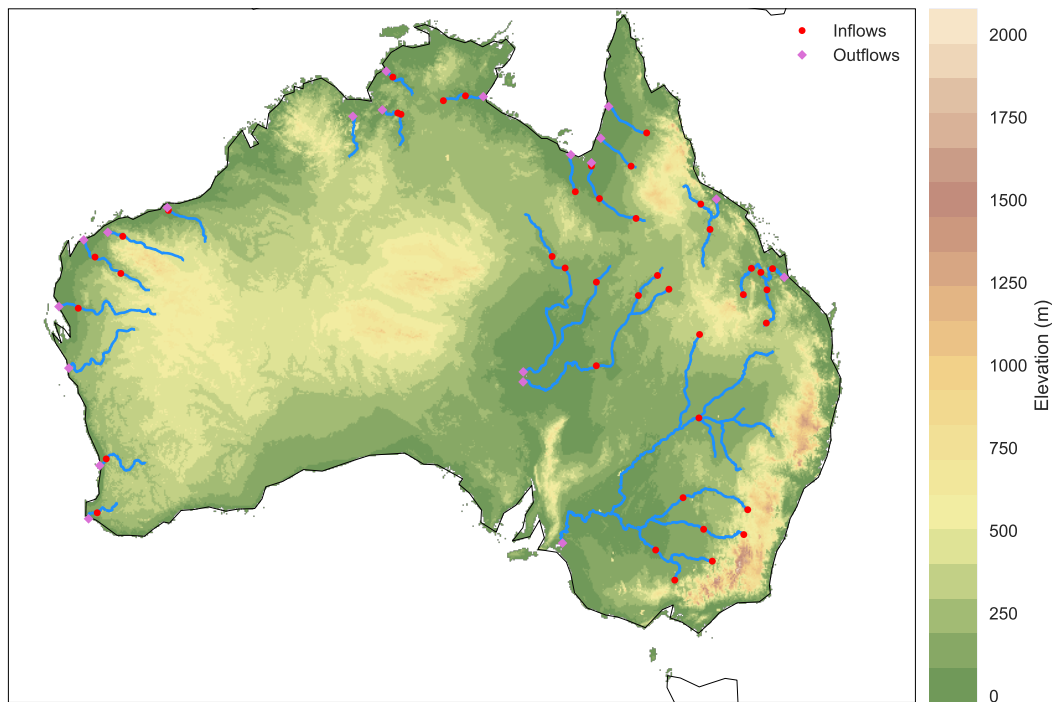


Figure S2. Map of the Australia model domain and its topography. Boundary inflows and outflows for the LISFLOOD-FP model are shown along with the modeled rivers.

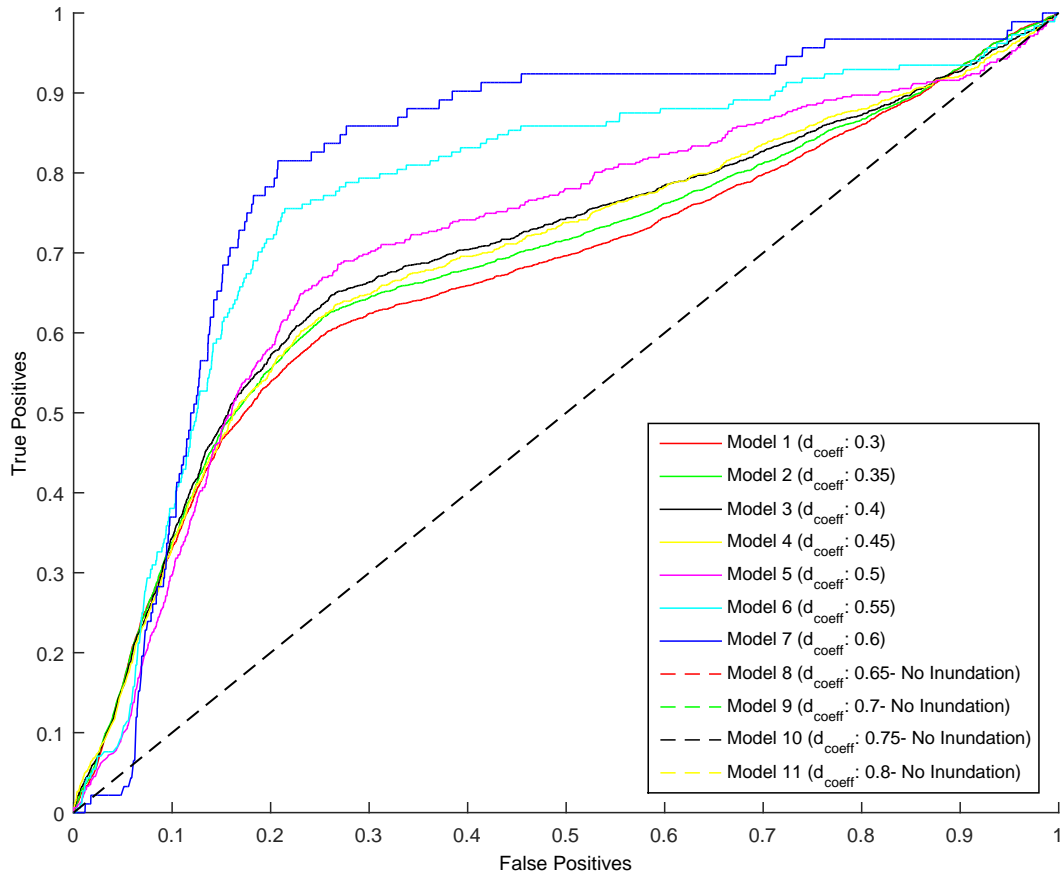


Figure S3. ROC curve obtained from comparison of optimized LISFLOOD-FP model-predicted and Landsat-observed flood inundation over a region of the Murray-Darling River basin.

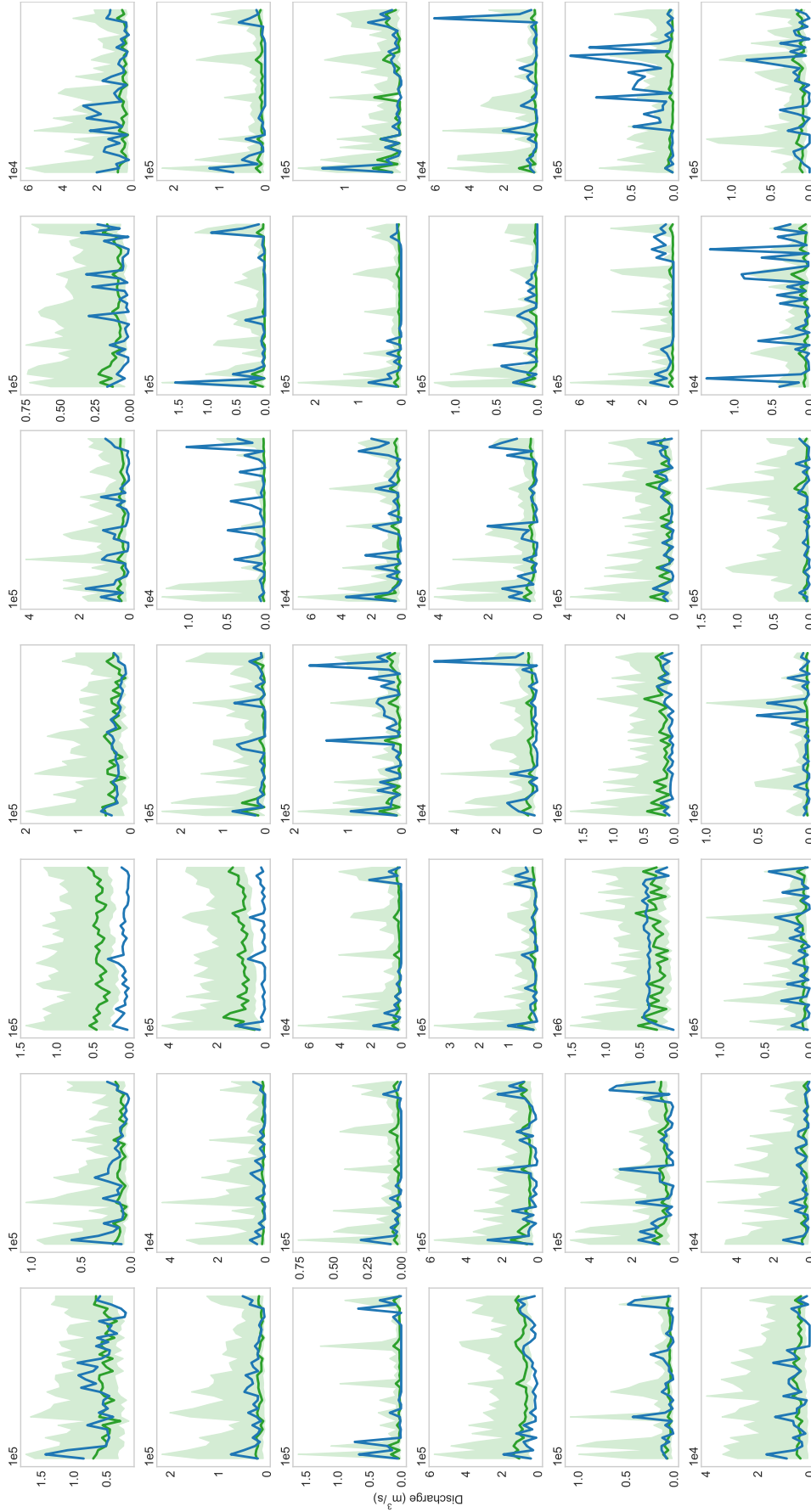


Figure S4. Annual (1973–2012) observed (blue line) and simulated (shown as the ensemble mean and spread in green) streamflow at each inflow location.

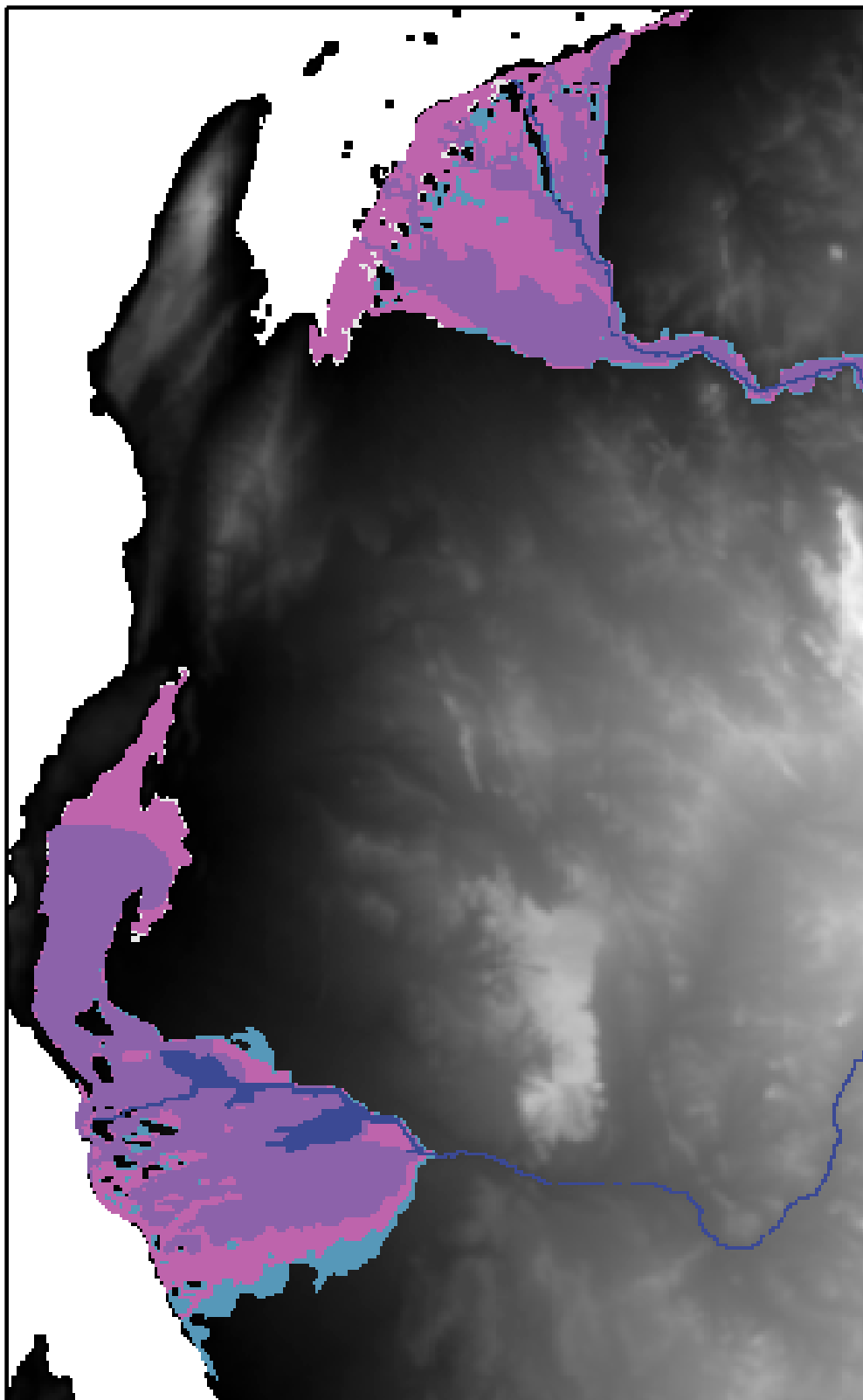


Figure S5. Bivariate choropleth map of agreement in maximum inundated area between the benchmark and reanalysis simulations during the 1973-2012 study period for western Australia.

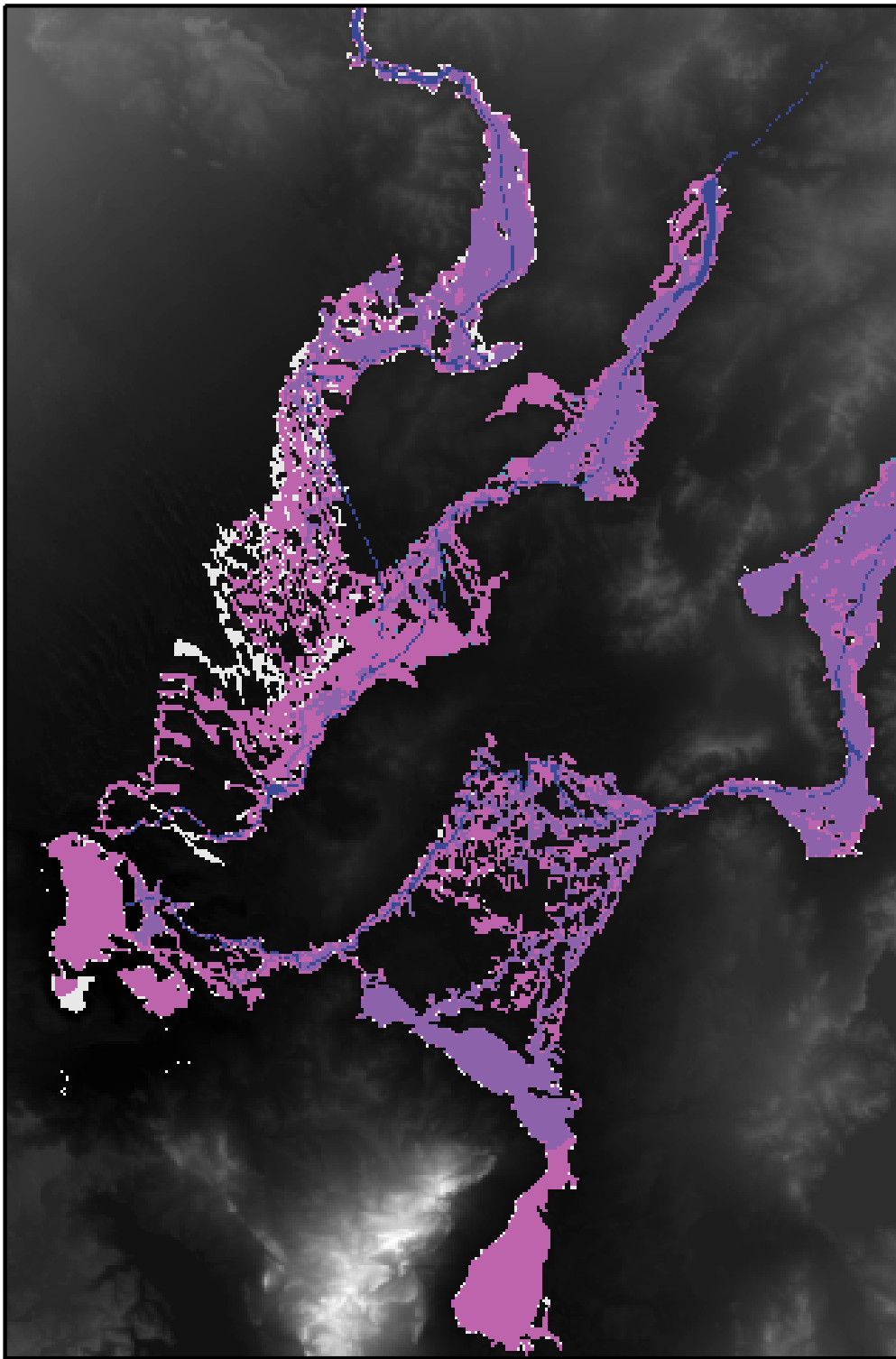


Figure S6. Same as Figure S5 for the Queensland region.

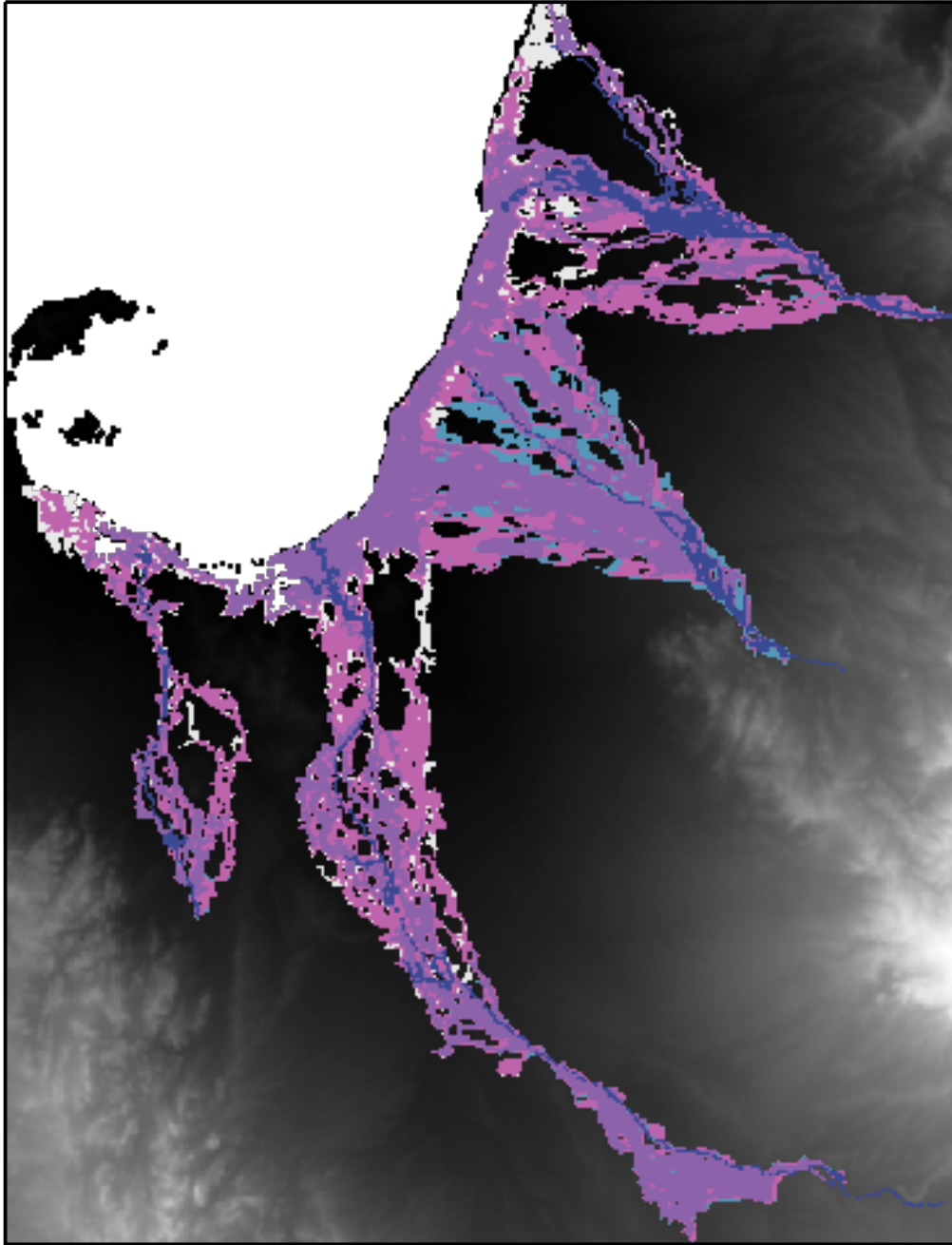


Figure S7. Same as Figure S5 for northern Australia.

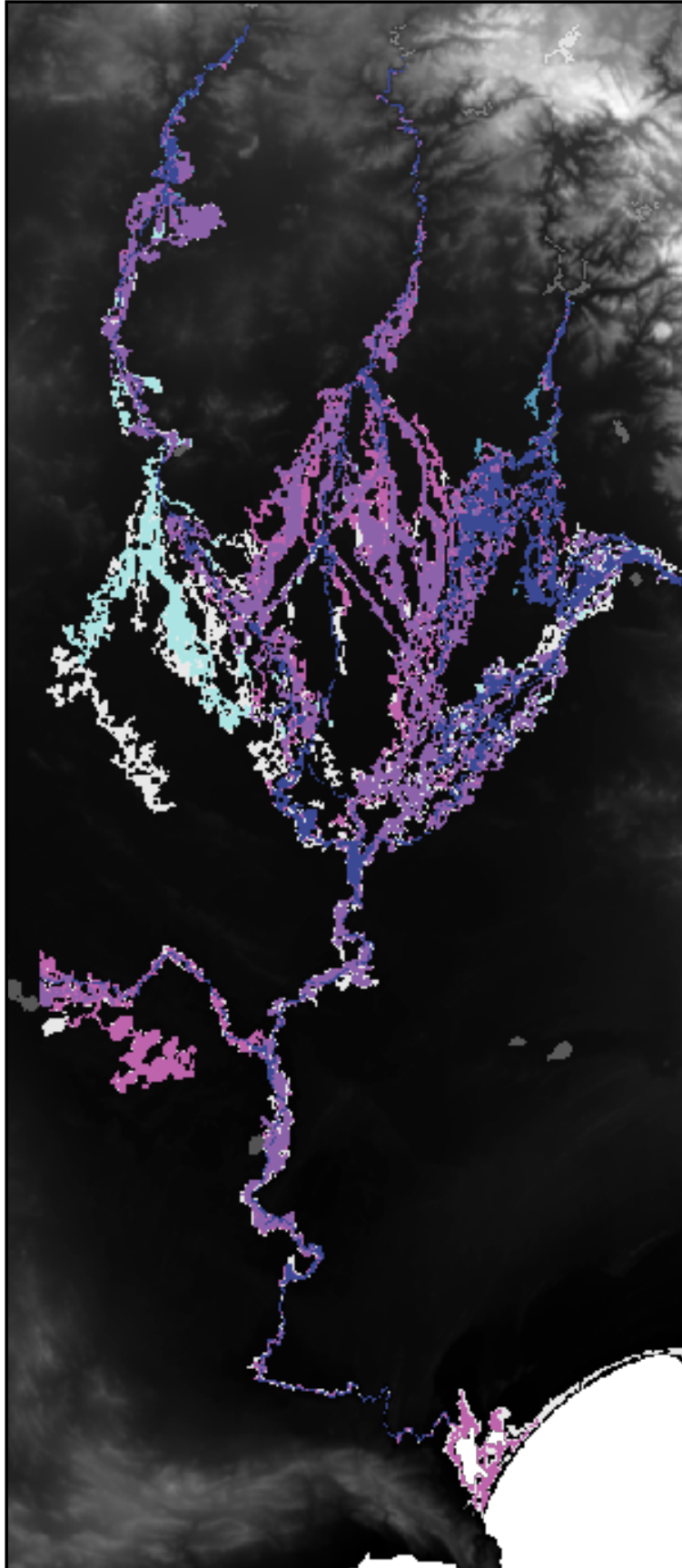


Figure S8. Same as Figure S5 for the Murray-Darling region.